Astron. Astrophys. 350, 197–203 (1999)

ASTRONOMY AND ASTROPHYSICS

Outflow and disk around the very young massive star GH2O 092.67+03.07

J.P. Bernard[1], **K. Dobashi**[2], **and M. Momose**[3]

[1] Institut d'Astrophysique Spatiale, bât 121, Campus d'Orsay, F-91405 Orsay Cedex, France
[2] Department of Astronomy and Earth Sciences, Tokyo Gakugei University, Koganei 184-8501, Tokyo, Japan
[3] Nobeyama Radio Observatory, National Astronomical Observatory, Nobeyama, Minamisaku, Nagano 384-1305, Japan

Received 6 October 1998 / Accepted 9 June 1999

Abstract. We present CS(J=2-1) interferometric observations obtained with the Nobeyama Millimeter Array (NMA) toward a protostar ($\mathrm{GH2O\,092.67+03.07}$) in the Cygnus OB7 giant molecular cloud (distance=800 pc). The data clearly indicate the presence of a compact (size $\simeq 8\,10^3$ AU) and young outflow with dynamical time scale $\simeq 3500$ year. The outflow is surrounded by a massive gas condensation. The analysis of the gas dynamics shows the signature of an infalling and rotating disk, which could be the first clear detection of such motion around a young high mass star. Single dish data obtained with the Nobeyama 45m antenna in several molecular lines are used to derive the CS abundance and the optical depth of the CS(J=2-1) toward $\mathrm{GH2O\,092.67+03.07}$. We derive a total mass of $\simeq 0.6\,\mathrm{M}_\odot$ and $\simeq 12\,\mathrm{M}_\odot$ for the outflow and disk respectively. The comparison of the NMA data with a simple model of infalling disk indicates a mass of the central object in the range $4.0 < M_* < 7.5\,\mathrm{M}_\odot$.

We propose that $\mathrm{GH2O\,092.67+03.07}$ is a dust condensation in the very early steps of forming a high mass star.

Key words: ISM: clouds – ISM: jets and outflows – stars: formation – stars: individual: GH2O 092.67+03.07

1. Introduction

The source $\mathrm{GH2O\,092.67+03.07}$ is located in the so called Northern Coal Sack region (NCS) within the giant molecular complex Cygnus OB7 ($\mathrm{l} \simeq 93°, \mathrm{b} \simeq 4°$) at $\mathrm{D} = 800\,\mathrm{pc}$ (Dame & Thaddeus 1985). The complex presents evidence for intermediate and high mass star formation. The large scale distribution of the dense molecular gas over the entire Cygnus region was studied in details by Dobashi et al. (1994). This ^{13}CO survey revealed that the mass of the dense gas over the entire complex Cygnus OB7 is about $7.7\ 10^4\,\mathrm{M}_\odot$. $\mathrm{GH2O\,092.67+03.07}$ appears as a bright millimeter and submillimeter continuum source located about 30″ south of a compact H II region ($\mathrm{IRAS21078+5211}$). The submillimeter continuum emission of $\mathrm{GH2O\,092.67+03.07}$ was first detected by Jenness et al. (1995), and the radio continuum emission from the H II region was mapped by McCutcheon et al. (1991). The millimeter source contains an $\mathrm{H_2O}$ maser (e.g. Miralles et al. 1994), a well known sign of stellar formation activity. VLA measurements of this maser (Jenness et al. 1995) have shown that its precise position ($\alpha_{1950} = 21^\mathrm{h}07^\mathrm{m}46.65^\mathrm{s}$, $\delta_{1950} = 52°10'22.8''$; l=92.67°, b=+3.07°) is consistent with that of the millimeter source, but falls outside the radio contours of the H II region.

We have obtained a large amount of millimeter and submillimeter continuum data (from $200\,\mu\mathrm{m}$ to 2.1 mm) toward $\mathrm{GH2O\,092.67+03.07}$ using a wide variety of instruments. This dataset, which will be presented in details in a subsequent paper, shows that the millimeter source and the nearby H II region $\mathrm{IRAS21078+5211}$ are actually two distinct objects but both belong to an extended and massive (total mass larger than $900\,\mathrm{M}_\odot$) dust envelope with a more or less hydrostatic density profile. The total bolometric luminosity of the envelope is $L_\mathrm{bol} \simeq 8\,10^3\,\mathrm{L}_\odot$ with $L_\mathrm{bol}/L_{\lambda<350\,\mu\mathrm{m}} \simeq 50$, well below the canonical limit for class 0 protostars (< 200: André et al. 1993). No infrared source is detected by deep $10\,\mu\mathrm{m}$ observations at the location of $\mathrm{GH2O\,092.67+03.07}$, which indicates very little hot dust emission and/or very high extinction toward the young stellar object. We have also made extensive molecular line observations toward $\mathrm{GH2O\,092.67+03.07}$ using the Nobeyama 45m telescope. Some molecular lines including CO(J=1-0) and CS(J=2-1) as well as emission lines of their isotopes (^{13}CO, C^{18}O, and C^{34}S) were used to map the gas distribution around the source. The intensity distribution of these lines sharply peaks at the position of $\mathrm{GH2O\,092.67+03.07}$, indicating a high concentration of matter toward the source. The excitation temperature measured in CO is about 50 K at the source position, which is much higher than toward normal molecular clouds ($\simeq 10\,\mathrm{K}$).

All these facts strongly indicate that massive star formation in a very early stage is taking place in the dense condensation $\mathrm{GH2O\,092.67+03.07}$. In this paper, we present the results of observations obtained toward $\mathrm{GH2O\,092.67+03.07}$ using the Nobeyama Millimeter Array (NMA) interferometer. We also use a subset of the 45m data (spectra obtained directly toward the source) in order to derive the CS abundance and the optical depth of the CS(J=2-1) line used with the interferometer. The data and data reduction are described in Sect. 2. The high an-

Send offprint requests to: J.P. Bernard (bernard@ias.fr)

gular resolution observations with the NMA allow to resolve a compact and young outflow, surrounded by a rotating and infalling disk which physical parameters are derived in Sect. 3. Our conclusions relative to the nature of $\mathrm{GH2O\,092.67+03.07}$ are summarized in Sect. 4.

2. Observations

The aperture synthesis observations were performed using Nobeyama Millimeter Array (NMA) in 1996 February. We employed SIS receivers (Sunada et al. 1993) which provided a typical system noise temperature of $\simeq 200\,\mathrm{K}$ (DSB) toward the zenith. An FFT spectrometer (Chikada et al. 1987) with 1024 frequency channels per baseline was used to obtain the spectral data. We applied an $80\,\mathrm{MHz}$ filter to the correlator, which resulted in $0.24\,\mathrm{km\,s^{-1}}$ velocity resolution at the CS(J=2-1) rest frequency of $98\,\mathrm{GHz}$. Continuum emission data at $98\,\mathrm{GHz}$ was simultaneously obtained using line-free frequency channels with an effective bandwidth of $55\,\mathrm{MHz}$. Observations were made with the C configuration (total 15 baselines). The minimum and maximum projected baseline lengths were 17 and 160 m respectively, for which our observations are insensitive to structures with spatial extent $> 38''$. The size of the synthesized beam is $3.4'' \times 3.0''$ with a position angle of 91°. Both phase and gain calibrations were made by observing BL-Lac every 40 minutes. The flux density of BL-Lac at $98\,\mathrm{GHz}$ was 3.3 Jy on February 1996 from observations of Uranus. We subtracted the continuum level from the visibility, and then applied the CLEAN algorithm in NRAO AIPS to each frequency channel. The rms noise level of the CS data is $1.1\,\mathrm{K}$ in one NMA beam at the velocity resolution of $0.24\,\mathrm{km\,s^{-1}}$, and that for the continuum data is 3.6 mJy/beam.

In order to determine the CS abundance and to estimate the total molecular mass detected with the NMA observations, we made additional observations in the CS (J=2-1) and $\mathrm{C^{34}S}$ (J=2-1) emission lines as well as in the CO(J=1-0), $^{13}\mathrm{CO}$ (J=1-0) and $\mathrm{C^{18}O}$ (J=1-0) lines toward $\mathrm{GH2O\,092.67+03.07}$ with the 45m telescope installed at NRO (HPBW=17″ at 110 GHz). The receiver used to obtain these data was an SIS receiver (S100) which provided a typical system noise temperature 350-500 K toward the zenith depending on the rest frequencies of the observed molecular lines (98-115 GHz). Spectrometers used for the 45m observations were acousto-optical spectrometers (AOSs) having a total bandwidth of $40\,\mathrm{MHz}$ with a frequency resolution of 40 kHz, corresponding to a velocity coverage and resolution of $\simeq 100\,\mathrm{km\,s^{-1}}$ and $\simeq 0.1\,\mathrm{km\,s^{-1}}$ at $\simeq 100\,\mathrm{GHz}$, respectively. The standard chopper-wheel method (Kutner & Ulich 1981) was used to scale the antenna temperature, which was finally converted to T_R^*, by applying the main beam efficiency of the telescope 0.50–0.55 at the observed frequencies. A few minutes integration was performed to obtain each spectra, which resulted in a typical rms noise of 0.2–1 K at the velocity resolution $0.1\,\mathrm{km\,s^{-1}}$ for all the spectra. The pointing accuracy of the observations was better than $\simeq 10''$ and was checked by observing the SiO maser source T Cep at $43\,\mathrm{GHz}$ every 2 hours. Here, we present only 45m data toward the central position of $\mathrm{GH2O\,092.67+03.07}$. The full maps obtained in several molecular transitions will be analyzed in a subsequent paper.

3. Results

3.1. Determination of the CS fractional abundance and the optical depth using single dish data

Our high angular resolution data obtained using the NMA is limited to the CS (J=2-1) transition emission line. In order to estimate the molecular mass distribution from the NMA data, we derive some physical parameters such as the excitation temperature, the optical depth, and the fractional abundance of the CS molecule in this subsection, using the spectra obtained toward $\mathrm{GH2O\,092.67+03.07}$ with the 45m single dish telescope. The quantities derived here are mostly based on the comparison of the column densities of CS and the carbon monoxide, because large variations of the CS fractional abundance have been observed in some molecular clouds, while that of CO and its isotopes are likely to remain more constant, not only over different regions but also in different stages of cloud evolution (e.g., Suzuki et al. 1992; Wiesemeyer et al. 1997). Therefore, we expect the comparison between the molecular transitions used here to allow a reliable estimate of the molecular mass distribution at the small NMA scales.

The spectra obtained using the 45m telescope, i.e., $^{12}\mathrm{CO}$ (J=1-0), $^{13}\mathrm{CO}$ (J=1-0), $\mathrm{C^{18}O}$ (J=1-0), CS(J=2-1), and $\mathrm{C^{34}S}$ (J=2-1) are displayed in Fig. 1. The faint emission component at $V_\mathrm{lsr} = 8\,\mathrm{km\,s^{-1}}$ seen as a shoulder in the $^{12}\mathrm{CO}$ spectrum likely belongs to the giant molecular cloud Cyg OB7 (Dobashi et al. 1994) lying along the same line of sight. High velocity wings, indicating the existence of a molecular outflow, are clearly evidenced in the $^{12}\mathrm{CO}$ spectrum. The red wing of the outflow is also detected in the CS and $^{13}\mathrm{CO}$ spectra. Physical parameters resulting from a least square fit using a single gaussian velocity component are summarized in Table 1. It is noteworthy that $\mathrm{GH2O\,092.67+03.07}$ exhibits a quite intense molecular emission especially in the optically thick $^{12}\mathrm{CO}$ line ($T_\mathrm{R}^*(^{12}\mathrm{CO}) = 47.8\,\mathrm{K}$). It is bright even in the CS line (12 K), which is generally no more than a few K in normal dark clouds at this angular resolution.

We derive column densities for the various species assuming LTE using,

$$N = \frac{C_0 T_\mathrm{ex}}{1-e^{-T_0/T_\mathrm{ex}}} \frac{e^{J_\mathrm{lev} T_0/2T_\mathrm{ex}}}{J_\mathrm{lev}+1} \frac{\beta^{-1}\int T_\mathrm{R}^*(v)dv}{J(T_\mathrm{ex})-J(2.7\,K)} \quad (1)$$

$$\simeq \frac{C_0 T_\mathrm{ex}}{1-e^{-T_0/T_\mathrm{ex}}} \frac{e^{J_\mathrm{lev} T_0/2T_\mathrm{ex}}}{J_\mathrm{lev}+1} \tau_0 \Delta V, \quad (2)$$

where $J(T) = T_0/(e^{(T_0/T)}-1)$. T_ex is the excitation temperature of the molecule, J_lev is the lower level of the transition and the parameters C_0 and T_0 are the constants listed in Table 1 for a given emission line. τ_0 is the optical depth at the peak velocity of the line ($v = V_\mathrm{lsr}$). β is the escape probability which is related to the beam and velocity averaged optical depth $\bar{\tau}$

Table 1. Properties mesured for the disk and outflow components derived from the 45m single dish data.

line	Constants		Observed Values			Derived Quantities					
	T_0	C_0	$T_{\rm R}^{*\flat}$	$V_{\rm lsr}$	$\Delta V^\flat$	Column Density $\rm cm^{-2}$		$\int T_{\rm R}^* dV$ $\rm K km\,s^{-1}$		τ_0	$\bar{\tau}$
	K	$\frac{\rm cm^{-2}K^{-1}}{\rm km\,s^{-1}}$	K	$\rm km\,s^{-1}$	$\rm km\,s^{-1}$	disk†	flow‡	disk	flow	disk	flow
^{12}CO (J=1-0)	5.53	$2.40\,10^{14}$	47.8	-6.9	3.5	–	$2.2(1.9)\,10^{17}$	178.8	37.3	$>>1$	2.0
^{13}CO (J=1-0)	5.29	$2.51\,10^{14}$	19.5	-6.3	2.8	$1.9\,10^{17}$	$2.4\,10^{15}$	59.2	0.9	0.52	0.02
C^{18}O (J=1-0)	5.27	$2.52\,10^{14}$	1.2	-6.1	2.7	$9.4\,10^{15}$	$< 4.7\,10^{14}$	3.7	< 0.17	0.002	$<<1$
CS(J=2-1)	4.70	$1.78\,10^{12}$	12.0	-6.2	3.8	$5.9\,10^{14}$	$5.9\,10^{13}$	48.1	5.3	0.287	0.01
C^{34}S (J=2-1)	4.63	$1.81\,10^{12}$	1.9	-5.9	2.3	$5.2\,10^{13}$	$< 8.8\,10^{12}$	4.8	$< 0.2^\sharp$	0.04	$<<1$
H_2 *						$5.6\,10^{22}$	$2.2(1.9)\,10^{21}$				
$X_{\rm CS}$						$1.1\,10^{-8}$	$2.7(3.0)\,10^{-8}$				

† The integration range for the disk is $-10 < V_{\rm lsr} < -2\,\rm km\,s^{-1}$.
‡ The integration range for the outflow is $-17 < V_{\rm lsr} < -10\,\rm km\,s^{-1}$ and $-2 < V_{\rm lsr} < 5\,\rm km\,s^{-1}$.
* From C^{18}O and ^{13}CO for the disk and outflow respectively.
$^\sharp$ upper limit detection derived from the noise level.
$^\flat$ $T_{\rm R}^*$ is measured at the peak velocity $V_{\rm lsr}$. ΔV is measured at FWHM.

as $\beta = (1 - e^{-\bar{\tau}})/\bar{\tau}$. Eq. 2 is the approximation for a purely Gaussian line, using

$$T_{\rm R}^*(v) = (J(T_{\rm ex}) - J(2.7\,K))(1 - e^{-\tau(v)}). \quad (3)$$

The excitation temperature $T_{\rm ex}$ is derived from the ^{12}CO emission spectrum using Eq. 3, under the assumption that the line is very optically thick (i.e. $1 - e^{-\tau_0} \simeq 1$), leading to a value of $T_{\rm ex} = 51.4\,\rm K$. Throughout this paper, we assume the same $T_{\rm ex}$ value for all the molecular lines observed. The optical depth for each line is then computed using Eq. 3 and the $T_{\rm R}^*$ values from Table 1. We then derive the column densities of each species using Eq. 2, ΔV from Table 1 and the optical depth derived above. These values are summarized in Table 1. We estimate the H_2 column density N(H_2) for the disk from $N(\rm C^{18}O)$, using the empirical relation $N(\rm H_2) = [N(C^{18}O)/1.8\,10^{14}{+}3.7)]\,10^{21}$ (Frerking et al. 1982). The comparison with $N(\rm C^{18}O)$ derived above leads to a fractional CS abundance $X_{\rm CS} = N(\rm CS)/N(H_2) = 1.1\,10^{-8}$, which stands for the average value normalized in the beam of the 45m telescope (HPBW$\simeq 17''$). It must be noted that the values derived above are averaged in one 45m beam. It is likely however that the CS emitting region is smaller than the beam, so that the optical depth value for the CS transition in Table 1 may largely underestimate the actual value. If we assume that CS and C^{34}S are emitted in the same region and set the ratio of column densities to match terrestrial abundance ($N(\rm CS)/N(C^{34}S)$=[CS]/[C^{34}S] = 22.6) using Eq. 1 under the hypothesis that $\bar{\tau}(\rm C^{34}S) << 1$, we obtain $\bar{\tau}(\rm CS) = 2.0$, significantly higher than the beam average value given in Table 1. We shall use this value, instead of the one in Table 1 when computing masses from our NMA data. We note also that the method used to derive $X_{\rm CS}$ for the disk assumed the same spatial distribution for the CS and C^{18}O molecules from which $N(\rm H_2)$ is derived. This is the major source of uncertainty upon $X_{\rm CS}$.

As clearly seen in the ^{12}CO spectrum (Fig. 1), we detect blue and red shifted high velocity components toward GH2O 092.67+03.07, which indicates the presence of a molecular outflow. As shown in the next subsection, the outflow is actually resolved by our NMA observations in CS, and intense blue and red shifted high velocity wings are detected towards GH2O $092.67 + 03.07$ in the velocity ranges $-17 < V_{\rm lsr} < -10\,\rm km\,s^{-1}$ and $-2 < V_{\rm lsr} < 5\,\rm km\,s^{-1}$ respectively (see Fig. 1 as well as the next subsection). Since it has been reported that the CS molecule is likely to be over-abundant in outflows (e.g. Tatematsu et al. 1993) which may be due to the destruction of dust grains, we determine the CS abundance in the outflow by comparing the CS column density and that of H_2 estimated from the ^{12}CO spectrum in the above velocity ranges.

We derive the optical depth of the ^{12}CO line in the outflow assuming terrestrial abundance ratio of the ^{12}CO and ^{13}CO lines (i.e. $N(^{12}\rm CO)/N(^{13}\rm CO) = [^{12}CO]/[^{13}CO] = 89.9$) and that $\bar{\tau}(^{13}\rm CO) << 1$ in the outflow. Eq. 1 then leads to $\bar{\tau}(^{12}\rm CO) = 2.0$. The ^{12}CO column density is then derived using Eq. 1. The same procedure is used with CS and C^{34}S, leading to $\bar{\tau}(CS) \simeq 0.01$ and the CS column density given in Table 1. The H_2 column density $N(\rm H_2)$ in the outflow wings is estimated from $N(^{12}\rm CO)$ assuming the ^{12}CO fractional abundance $N(^{12}\rm CO)/N(H_2)$=1 10^{-4} (Frerking et al. 1982). The CS molecule abundance derived in the outflow is $X_{\rm CS} = 2.7\,10^{-8}$.

3.2. Outflow and disk physical parameters

Fig. 2 shows some typical CS(J=2-1) spectra obtained using the NMA interferometer. Note the unusually high antenna temperature ($\simeq 30\,\rm K$) which makes GH2O $092.67 + 03.07$ one of the brightest known sources on the sky at the NMA scale (almost as bright as the calibration source Orion KL). The dip around $-6.0\,\rm km\,s^{-1}$ corresponds to the systemic velocity of the more extended cloud detected in our 45m data, but the intensity, at the scales which are resolved-out by the interferometer ($> 38''$), is only about 3 K in our 45m data. It is therefore unlikely that the

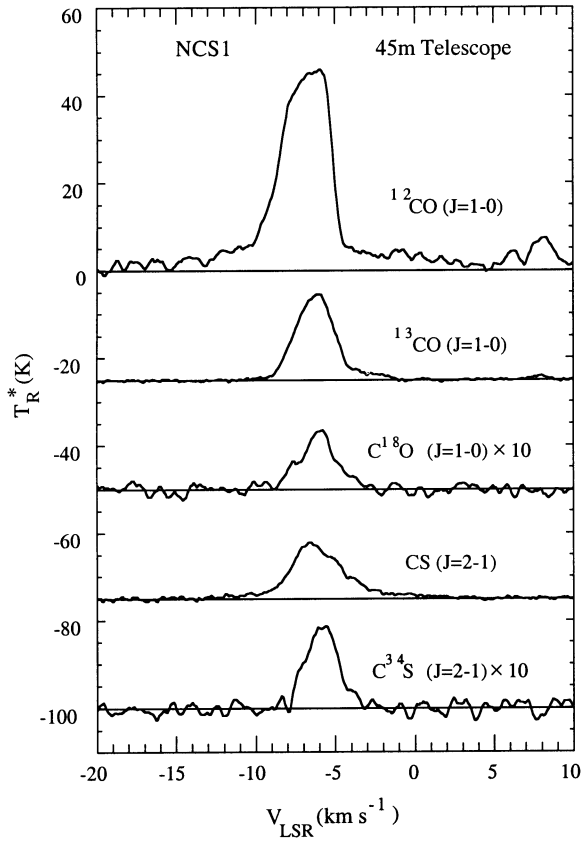

Fig. 1. Molecular emission lines observed toward GH2O 092.67 + 03.07 using the NRO 45m telescope. Intense emission lines are observed in ^{12}CO ($\simeq$ 50 K), ^{13}CO ($\simeq$ 20 K) and CS ($\simeq$ 12 K). The ^{13}CO, C^{18}O, CS and C^{34}S spectra are offset by -25 K, -50 K, -75 K, and -100 K, respectively. The weaker C^{18}O and C^{34}S spectra are magnified 10 times in the figure.

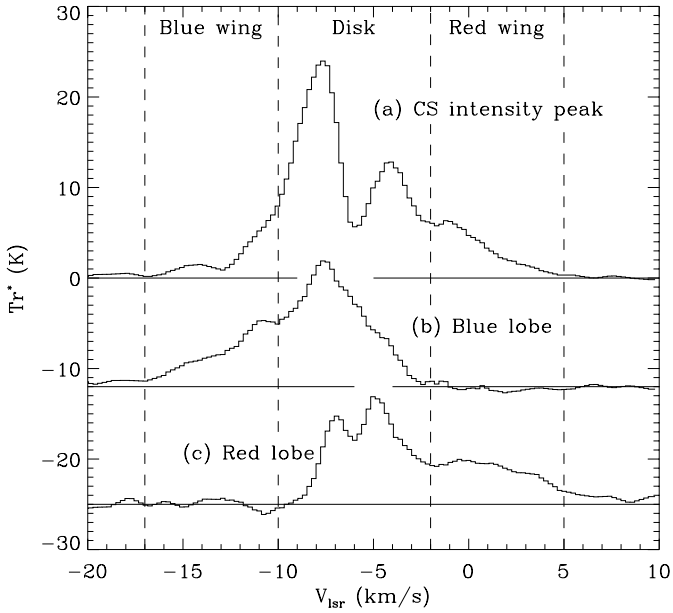

Fig. 2. NMA spectra obtained around GH2O 092.67 + 03.07 in the CS(J=2-1) line: (a) at the intensity peak position (α_{1950} = $21^h07^m46.60^s$, δ_{1950}= 52°10′23.3″) (b) at the intensity peak position of the outflow blue lobe (α_{1950} = $21^h07^m46.11^s$, δ_{1950}=52°10′21.8″) (c) Same as (b) for the red lobe (α_{1950} = $21^h07^m47.35^s$, δ_{1950}=52°10′24.5″). The velocity resolution has been smoothed down to 0.96 km s^{-1}. The velocity intervals used for the disk and outflow lobes are shown.

resolved-out component contributes most of the dip observed toward the central regions. Self-absorption of the CS(J=2-1) line in the densest regions of our map could possibly explain the observed dip. However, it is also likely that the interferometer selectively detects dense circumstellar material and the spectral structure observed could also reflect systematic motion in the protostellar envelope (see Sect. 3.3). A full reconstruction of spatial frequencies with the help of our 45m data as well as additional NMA observations in thinner molecular lines are forseen, in order to help disentangle from the effects described above.

The compact outflow detected in one beam of the 45m telescope is resolved by the present interferometric CS observations. The outflow lobes are found to extend $\simeq 10''$ away from the peak intensity position of the continuum emission, where the central star is most likely forming. On the basis of the CS data, we determined the velocity ranges for the blue and red shifted high velocity wings to be $-17 < V_{\rm lsr} < -10\,{\rm km\,s^{-1}}$ and $-2 < V_{\rm lsr} < 5\,{\rm km\,s^{-1}}$, respectively. Fig. 3a shows the CS distribution of the outflow integrated over those velocity intervals. The rest of the CS emission ($-10 < V_{\rm lsr} < -2\,{\rm km\,s^{-1}}$) stands for the dense gas surrounding GH2O 092.67 + 03.07 and is supersposed on the outflow contours in the figure. Hereafter, we shall refer to this component as disk. The 98 GHz continuum data is shown in Fig. 3b at the same scale. It is tracing dust emission in the dense disk structure and exhibits an elliptical shape with its major axis orthogonal to the outflow elongation, which agrees with the geometry expected for an outflow-disk system around protostars. On the other hand, the CS disk is more round with an intense ridge across the interface between the outflow and the disk (see the northern flank of the outflow lobes). This feature is often observed toward protostars, and can be attributed either to the increasing density of gas that has been swept up by the outflow (e.g., Momose et al. 1996, Dobashi et al. 1998) or to the CS abundance enhancement through the destruction of dust grains by the outflow (e.g. Tatematsu et al. 1993, Mikami et al. 1992). Actually, the mean CS abundance $X_{\rm CS} = N({\rm CS})/N({\rm H_2})$ is estimated to be $1.1\,10^{-8}$ around GH2O 092.67 + 03.07 from our 45m observations, which is about one order of magnitude higher than in nearby dark clouds (Frerking et al. 1980). An even higher abundance of $X_{\rm CS} = 2.7\,10^{-8}$ is observed in the outflow lobes.

The CS column density $N({\rm CS})$ was obtained from the interferometer data using Eq. 1 and the optical depth for the CS(J=2-1) transition and abundances of the CS molecule derived in Sect. 3.1 using the 45m data. The masses derived for the disk and the outflow (using a mean molecular weight of 2.4 times the proton mass) are 12.0 and $0.6\,{\rm M_\odot}$ respectively (see Table 2). Note that the outflow is rather massive with a

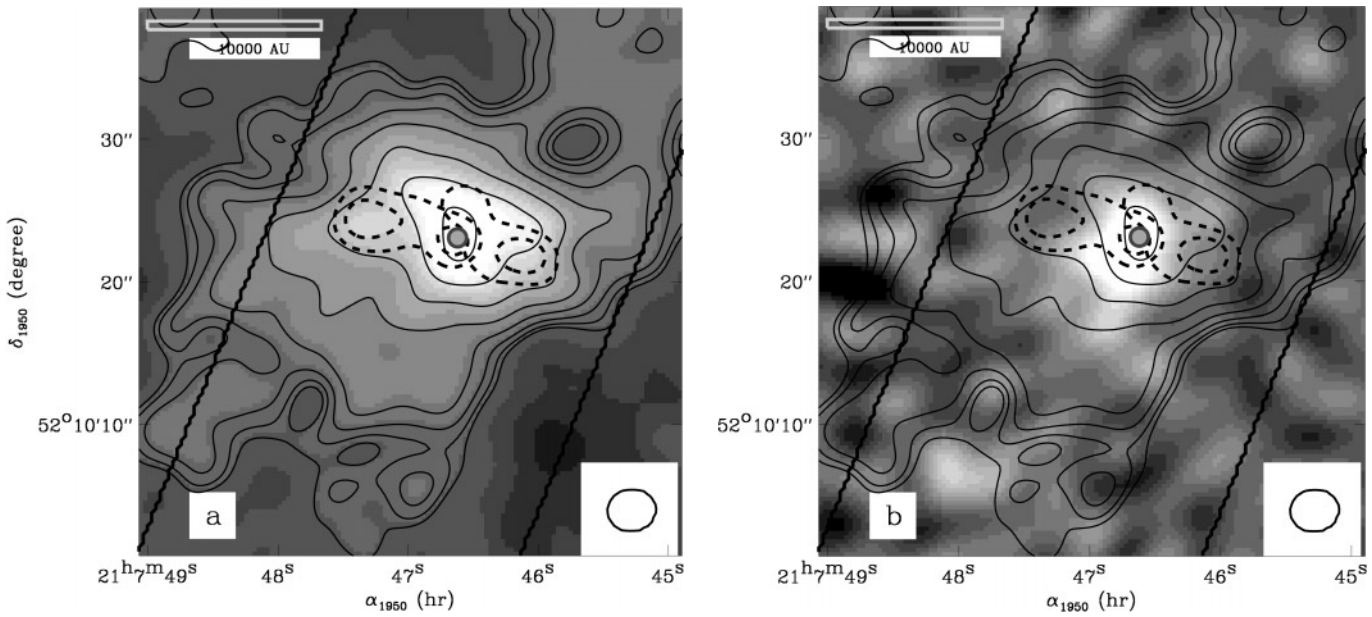

Fig. 3. **a** Integrated intensity distribution around GH2O 092.67 + 03.07 in the CS(J=2-1) disk component (grey). **b** Continuum emission distribution (grey). In both figures, the solid contours represent the CS(J=2-1) integrated intensity ($\mathrm{Kkm\,s^{-1}}$) in the velocity range for the disk (see Table 2) in log scale starting from 0.6 with steps of 0.2. The dashed contours for the ouflow component correspond to 15 and $25\,\mathrm{Kkm\,s^{-1}}$ for both the blue (west) and red (east) lobes. The beam size and linear scale at D =800 pc is shown. The dot central is the most likely position of the central star. The strip used to produce Fig. 4 is shown.

Table 2. Outflow and disk parameters derived from NMA interferometric data

	Outflow	Disk
$N(\mathrm{H_2})\,(\mathrm{cm^{-2}})$	–	$2.45\,10^{23}$
$R(''$ [AU])	10 [$8.0\,10^3$]†	$R_\mathrm{d} = 9$ [$7.2\,10^3$]$^\sharp$
$n(\mathrm{H_2})\,(\mathrm{cm^{-3}})$	–	$1.87\,10^{6\flat}$
$M(\mathrm{M_\odot})$	0.6	12.0
$v(\mathrm{km\,s^{-1}})$	$-17 < \mathrm{V_{lsr}^{blue}} < -10$	$v_\mathrm{rot} = 1.2^{+0.36\star}_{-0.24}$
	$-2 < \mathrm{V_{lsr}^{red}} < 5$	$v_\mathrm{inf} = 1.9 \pm 0.95^\star$
τ_dyn (yr)	$3.5\,10^{3\ddagger}$	$1.2\,10^4$
$\dot{M}(\mathrm{M_\odot\,yr^{-1}})$	$1.7\,10^{-4}$	$1.0 \pm 0.5\,10^{-3}$
$L(\mathrm{L_\odot})$	0.38	$2\,10^4 - 1.\,10^5 = L_\mathrm{ac}$
$\mathcal{M}\,(\mathrm{M_\odot\,km\,s^{-1}})$	3.3	–
$E(\mathrm{M_\odot(km\,s^{-1})^2})$	12.0	–

† Maximum distance of the outflow lobes from the center.
‡ $\tau_\mathrm{dyn} = \mathrm{R/V_{char}}$ where $V_\mathrm{char} = 11\,\mathrm{km\,s^{-1}}$ is the maximum outflow velocity measured from the mean velocity of the ambient gas ($V_\mathrm{lsr} = -6.0\,\mathrm{km\,s^{-1}}$).
$^\sharp$ at the FWHM contour level of the CS intensity distribution.
$^\flat$ $n(\mathrm{H_2}) = N(\mathrm{H_2})/R_\mathrm{d}$.
* values at $r = R_\mathrm{d}$. Quoted errors correspond to the 70% confidence level.
All values assume $i = 45°$.

very low dynamical time scale of only $3.5\,10^3$ yr. Although this time scale may significantly underestimate the actual age of the outflow, in particular if the outflow expanssion is slown down by dense regions in the envelope, the low value indicates that GH2O 092.67 + 03.071 is presently in the very early stage of stellar formation. The time scale and the mass yields an estimate for the mass loss rate of $\dot{M} = 1.7\,10^{-4}\,\mathrm{M_\odot\,yr^{-1}}$, which is much higher than usual for low-mass young stars ($\dot{M} = 10^{-5} - 10^{-8}\,\mathrm{M_\odot\,yr^{-1}}$: Levreault 1985), but comparable to those of massive young stars such as IRAS22142+5206 ($M_* \simeq 17\,\mathrm{M_\odot}$, $\dot{M} = 1.0\,10^{-4}\,\mathrm{M_\odot\,yr^{-1}}$: Dobashi et al. 1998) and GL490 ($M_* \simeq 13\,\mathrm{M_\odot}$, $\dot{M} = 1.5\,10^{-3}\,\mathrm{M_\odot\,yr^{-1}}$: Nakamura et al. 1991, Lada & Harvey 1981).

3.3. Disk dynamics

Fig. 4 shows the position-velocity map obtained by averaging our NMA data into a strip orthogonal to the outflow direction ($25''$ wide, oriented $22°$ relative to the North). The intensity distribution in the map is similar to the predictions of the simple model proposed by Ohashi et al. (1997) of a rotating and infalling disk. In particular, such a model naturally explains the overall assymetry of the map (caused by rotation) and the presence of two well defined emission peaks near the center (caused by infall). Following Ohashi et al., the rotation and infall velocities are assumed to follow $v_\mathrm{rot} \propto r^{-1}$ (conservation of the original angular momentum of the contracting cloud) and $v_\mathrm{inf} \propto r^{-0.5}$ respectively. The disk density is assumed to follow $n \propto r^{-1.5}$ and we used an external radius for the disk of $1.5\,10^4$ AU. Using this simplified model, we produced position-velocity maps for a set of infall and rotation velocities. The model predictions were then convolved with the response of the beam and velocity resolution of the NMA for a turbulence broadened FWHM velocity width of the line of $1\,\mathrm{km\,s^{-1}}$. The best match between the model predictions and

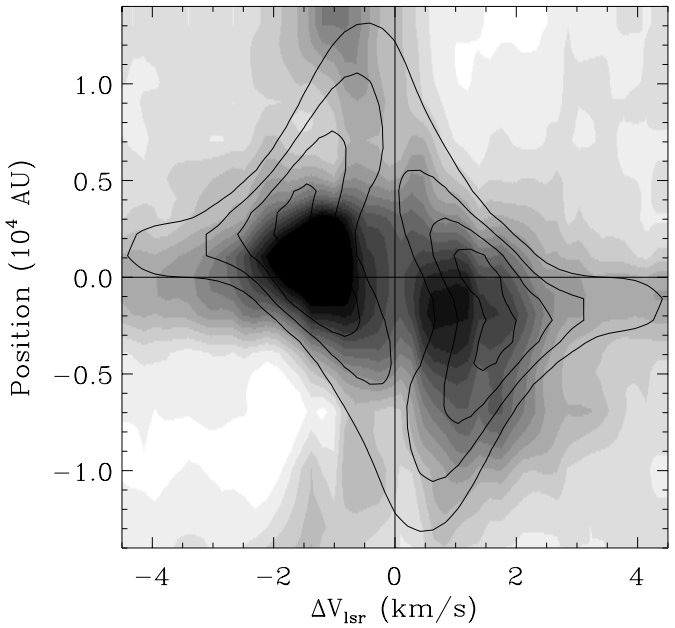

Fig. 4. Position-velocity map of the CS(J=2-1) data around $\mathrm{GH2O\,092.67+03.07}$ (grey scale) within a $25''$ strip along the disk (22°from North). The contours represent the best χ^2 fit to the data using the model described in the text. $\Delta V_{\rm lsr}$=0 corresponds to $V_{\rm lsr} = -6.0\,\mathrm{km\,s^{-1}}$.

our data was found by minimizing the χ^2, leaving $v_{\rm inf}$, $v_{\rm rot}$ as well as the position of the source in Fig. 4 as free parameters. The best χ^2 fit values normalized to $R_{\rm d} = 7.2\,10^3$ AU are $v_{\rm rot} = 1.2^{+0.4}_{-0.2}\,\mathrm{km\,s^{-1}}$ and $v_{\rm inf} = 1.9 \pm 0.9\,\mathrm{km\,s^{-1}}$ assuming a disk inclination of $\mathrm{i} = 45°$ (see Table 2). The position-velocity map for the model with these values is overlaid as contours in Fig. 4. It can be seen that the model reproduces reasonably well the overall structure of the observed velocity map. We note that, if the rotation is interpreted as Keplerian motion, the derived mass $M_{\rm kepl}(r < R_d) = 11.7^{+7.0}_{-4.7}\,\mathrm{M_\odot}$ is compatible with the disk mass derived from the NMA CS data ($M = 12\,\mathrm{M_\odot}$). Since this value is derived from the dynamics of the disk only and does not rely on the CS molecule abundance, the good agreement with the value derived from the CS emission is taken as a confirmation that our estimate of the CS abundance in the disk using the 45m data is in fact fairly accurate. With the disk parameters derived above, the time for a piece of the disk at r=$R_{\rm d}$ to collapse onto the central star is $\tau^{\rm disk}_{\rm dyn} = 1.2\,10^4$ yr, leading to an average infall rate of $\dot{M}_{\rm disk} = 1.0\,10^{-3}\,\mathrm{M_\odot\,yr^{-1}}$. Inversely, assuming that infall is steady over the dynamical time scale of the outflow we obtain a total accreted mass of $0.6\,\mathrm{M_\odot}$. Taking into account the mass ejected away by the outflow over the same time scale ($0.6\,\mathrm{M_\odot}$) leads to an estimated mass M_* in the range 4.1 to $7.4\,\mathrm{M_\odot}$ for the central object, where the range is derived from the errors on the infall and rotational velocities. The accretion luminosity, computed as $L_{\rm ac} = GM_*\dot{M}/R_*$ (with $R_* = 3.4\,\mathrm{R_\odot}$) falls in the range $L_{\rm ac} = 2\,10^4 - 1\,10^5\,\mathrm{L_\odot}$. This value can be compared with the bolometric luminosity of the dust envelope surrounding the protostar, as measured from our continuum submillimeter and millimeter measurements (down to $\lambda = 1.2\,\mathrm{mm}$). The total bolometric luminosity of the source is $\simeq 8\,10^3\,\mathrm{L_\odot}$, which includes the contribution from the compact H II region IRAS21078+5211($L = 3.3\,10^3\,\mathrm{L_\odot}$ assuming D=800 pc: Wouterloot & Brandt 1989) leading to $L_{\rm bol} = 4.7\,10^3\,\mathrm{L_\odot}$ for the contribution of $\mathrm{GH2O\,092.67+03.07}$ alone. The accretion luminosity derived above is therefore 4-20 times lower than the bolometric luminosity. Such a descrepancy ($L_{\rm ac} < L_{\rm bol}$) has already been evidenced for young massive objects (e.g. GL490, Nakamura et al. 1991). At the NMA scale, the accretion luminosity derived is relevant of the envelope material piling up into the disk. The discrepancy could then reflect that the overall accretion is a non steady process (as proposed by Hayashi et al. 1993) and that the actual accretion from the disk to the stellar surface, which cannot be observed directly at the NMA scale, occurs at a much lower rate than the envelope accretion at present time.

4. Conclusion

The interferometer data presented here have allowed to detect a very young bipolar outflow embedded in a thick rotating and infalling disk around the high mass protostar candidate $\mathrm{GH2O\,092.67+03.07}$. The masses of the outflow and disk are estimated to be 0.6 and $12\,\mathrm{M_\odot}$ respectively. Although the outflow is still very young (dynamical time scale of $\simeq 3.5\,10^3$ yr), its mass loss rate ($2.0\,10^{-4}\,\mathrm{M_\odot\,yr^{-1}}$) is among the highest known to date. The infall rate derived from the dynamics of the material surrounding the central object at the scale of 10^4 AU and the dynamical age of the outflow suggest that the central object may already have reached a mass of $\simeq 6\,\mathrm{M_\odot}$.

We propose that $\mathrm{GH2O\,092.67+03.07}$ is presently in the very early stage of forming a massive star. Over the few objects of this class known to date, $\mathrm{GH2O\,092.67+03.07}$ has the advantage of being very young and relatively nearby (800 pc) with a favorable geometry on the sky. An extensive observational study of the continuum and molecular emission on larger scale will be presented in forthcoming publications.

Acknowledgements. This work was financially supported by JSPS Fellowship for Research in Japan (No. S98032), and also partly funded by Grant-in-Aid for Scientific Research from the Japanese Ministry of Education, Science, and Culture (Nos. 10147204 and 11740122) as well as Sasagawa Scientific Research Grant from the Japan Science Society (No. 10–082).

References

André Ph., Ward-Thompson D., Barsony M. 1993, ApJ 406, 122
Chikada Y., Ishiguro M., Hirabayashi H. et al. 1987, Proc. IEEE, 75, 1203
Dame T.M., Thaddeus P. 1985, ApJ 297, 751
Dobashi K., Bernard J.P., Yonekura Y., Fukui Y. 1994, ApJS 95, 419
Dobashi K., Yonekura Y., Hayashi Y., Sato F., Ogawa H. 1998, AJ, 115,777
Frerking M. A., Wilson R. W., Linke R. A. 1980, ApJ, 240, 65
Frerking M. A., Langer W.D., Wilson R. W. 1982, ApJ, 262, 590
Hayashi M., Ohashi N., Miyama S. 1993, ApJ 418, L71

Jenness T., Scott P.F, Padman R. 1995, MNRAS 276, 1024
Kutner M. L., Ulich B. L. 1981 ApJ, 250, 341
Lada C. J., Harvey P. M. 1981, 245, 58
Levreault R. M. 1985, Ph.D. Thesis (Texas Univ., Austin.)
McCutcheon W.H., Dewdney P.E., Purton C.R., Sato P. 1991, ApJ 101, 1435
Mikami H., Umemoto, T., Yamamoto, S., Saito, S. 1992, ApJ, 392, L87
Miralles M.P., Rodríguez L.F, Scalise E. 1994, ApJS 92, 173
Momose M., Ohashi. N., Kawabe R., Hayashi M., Nakano T. 1996, ApJ, 470, 1001
Nakamura A., Kawabe R., Kitamura Y., Ishiguro M., Murata Y., Ohashi N. 1991, ApJ, 383, L81
Ohashi N., Hayashi Y., Ho P. T. P. et al. 1997, ApJ, 475, 2110
Sunada K., Kawabe R., Inatani J. 1993, Int. J. Infrared Millimeter Waves, 14, 1251
Suzuki H., Yamamoto S., Ohishi M., Kaifu N., Ishikawa S., Hirahara Y., Takano S. 1992, ApJ, 392, 551
Tatematsu K., Umemoto T., Murata Y., Chen H., Hirano N., Takaba H. 1993, ApJ, 419,476
Wiesemeyer H., Güesten R., Wink J. E., Yorke H. W. 1997, A&A, 320,287
Wouterloot J.G.A., Brand J. 1989, A&AS, 80,1149